Journal of
Instrumentation



# Spatial resolution characterization of a clinical Photon Counting Computed Tomography

To cite this article: Francesca Saveria Maddaloni *et al* 2026 *JINST* **21** C01018

*J inst*

PUBLISHED BY IOP PUBLISHING FOR SISSA MEDIALAB

RECEIVED: *September 30, 2025*
REVISED: *December 9, 2025*
ACCEPTED: *December 22, 2025*
PUBLISHED: *January 19, 2026*

26TH INTERNATIONAL WORKSHOP ON RADIATION IMAGING DETECTORS
BRATISLAVA, SLOVAKIA
6–10 JULY 2025

# Spatial resolution characterization of a clinical Photon Counting Computed Tomography

**Francesca Saveria Maddaloni**,[a,b,*] **Antonio Sarno**,[a] **Alessandro Loria**,[b] **Anna Piai**,[b] **Cristina Lenardi**,[a] **Antonio Esposito**[c] **and Antonella del Vecchio**[b]

[a] *Dipartimento di Fisica 'Aldo Pontremoli', Università degli Studi di Milano & INFN Sezione di Milano, via Celoria 16, 20133 Milano, Italy*

[b] *Medical Physics Department, IRCCS San Raffaele Hospital, via Olgettina, 60, 20132 Milano, Italy*

[c] *Advanced Center for Experimental Imaging, IRCCS San Raffaele Scientific Institute, Via Olgettina, 60, 20132 Milano, Italy*

*E-mail:* francesca.maddaloni@unimi.it

ABSTRACT: Computed Tomography (CT) is a cornerstone of diagnostic imaging but conventional systems, equipped with energy-integrating detectors (EIDs), present limitations in spatial resolution, noise, and tissue contrast. Photon-Counting CT (PCCT) addresses these limitations using photon-counting detectors (PCDs) that directly convert incoming X-ray photons into electric signals, enabling energy discrimination, material quantification, and virtual monoenergetic image reconstruction. Clinical applications have already included cardiovascular, thoracic, and neuroimaging examinations.

We performed a characterization of the spatial resolution of the first clinical PCCT scanner, the Naeotom Alpha® (Siemens Healthineers), equipped with CdTe PCDs. High-contrast presampled Modulation Transfer Function (MTF) was measured using a custom-built tungsten wire phantom tilted by 3°. Spatial resolution in radial and tangential was evaluated by shifting the phantom within the field of view. Three acquisition protocols were tested (head, abdomen/thorax, inner ear), including standard and Ultra-High Resolution (UHR) modes. Images were reconstructed with multiple iterative algorithms and kernels, and MTF analysis was automated via Python.

Results showed that spatial resolution increases with sharper reconstruction kernels across all anatomical protocols, with negligible differences between standard and vascular algorithms. UHR mode significantly improved resolution in the inner ear protocol ($f_{50\%}$ from 0.56 to 0.73 mm$^{-1}$; $f_{10\%}$ from 0.87 to 1.09 mm$^{-1}$).

*Corresponding author.



https://doi.org/10.1088/1748-0221/21/01/C01018

2026 JINST 21 C01018

In conclusion, this work provides an initial assessment of PCCT spatial resolution for acquisition protocols and reconstructions usually adopted in clinical routine. Future investigations will employ standardized phantoms and comparisons with other CT systems to further validate performance and assess its potential to enhance diagnostic imaging quality.

Keywords: Computerized Tomography (CT) and Computed Radiography (CR); X-ray detectors; Image reconstruction in medical imaging; Large detector-systems performance

2026 JINST 21 C01018

## Contents



2026 JINST 21 C01018

## 1 Introduction

Computed Tomography (CT) is an integral part of contemporary medicine. Conventional CT scanners are equipped with Energy Integrating Detectors (EID), which are based on the indirect conversion of the incoming photons into an electric signal for image generation. The signal, in this case, is related to the total energy fluence over the acquisition period. EID-based CT shows limitations regarding spatial resolution, noise, and tissue contrast [1]. A turning point of the actual CT technology is reached by the introduction of Photon-Counting CT (PCCT), which embodies Photon-Counting detectors (PCDs) in substitution of EIDs. PCDs are characterized by a semiconductor layer, usually cadmium telluride (CdTe) or cadmium zinc telluride (CZT), where the x-ray photons are absorbed, generating electron-hole pairs that are collected by pixelated anodes. The resulting signal is proportional to the absorbed photon energy, and a reading logic based on a calibrated threshold allows for the distinction and counting of detected photons. The final pixel value into the acquired projection reflects the number of detected photons, and the use of multiple thresholds also permits to include the photon energy in a specific energy bin. By means of dedicated software, this allows the quantitative estimation of material concentrations within the acquired object or patient and the generation of virtual monocromatic images (VMI), at all the energies of the incident X-ray spectrum. State-of-the-art clinical applications of PCCT regard cardiovascular exams, thoracic and lung imaging, and neuroimaging [2]. In this work, we characterized the first clinical cleared PCCT in terms of spatial resolution performance, namely the Naeotom Alpha® (Siemens Healthineers) equipped with CdTe PCDs.

## 2 Materials and methods

The PCCT scanner is equipped with two Vectron® X-ray tubes and two QuantaMax® photon-counting detectors. The declared in-plane spatial resolution is 0.11 mm and the z-coverage can be set to 144×0.4 mm or to 120×0.2 mm (Ultra-High Resolution). The spatial resolution of the PCCT scanner was characterized in terms of its high-contrast presampled Modulation Transfer Function (MTF). This function quantifies the system response to an impulsive input in the transformed Fourier domain [3]. An in-house phantom was realized to measure the MTF: it consisted of a thin tungsten (purity of 99.95%) wire, with a diameter of 12.5 µm. The phantom was realized so that the wire was very stretched between the two supports, and so that it could be easily aligned into the CT gantry. Figure 1 shows the in-house wire phantom.

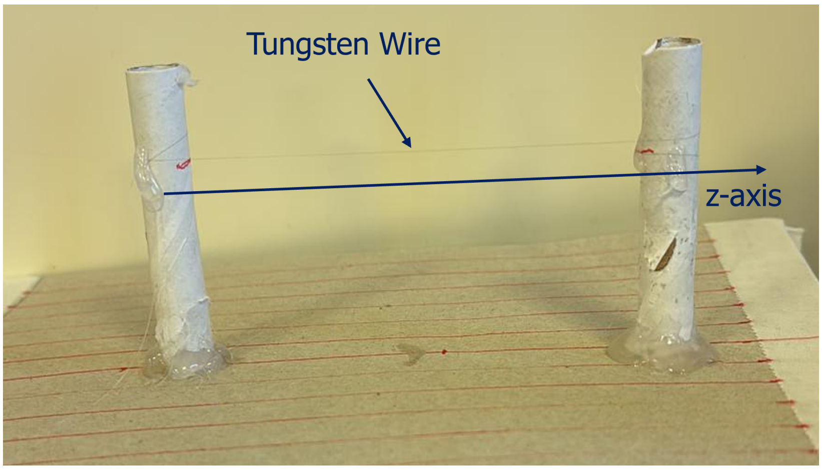


**Figure 1.** Picture of the in-house wire phantom for the measurement of the MTF. The length of the wire sample in the longitudinal direction was about 10 cm. The red lines were used to correctly align the wire into the CT gantry. The reference system is indicated: the wire was positioned with its length parallel to the patient longitudinal axis.

The wire was positioned in the CT gantry so that it was tilted at an angle of 3° with respect to the longitudinal axis (z-axis) of the scanner. This allows the determination of the presampled MTF, which is a validated method to avoid the aliasing of the digital detector system.

To characterize the spatial resolution dependence on the spatial direction, the line spread function generated from the image of the wire was presampled in radial direction (i.e., the direction connecting the axis of rotation and the periphery of the field of view) and along the tangential direction (i.e., the direction perpendicular to the radial direction and to the axis direction). For this reason, the wire was tilted either in the coronal plane or in the sagittal plane. Additionally, the dependence of the spatial resolution on the position within the field of view was investigated by repeating the measurements with the wire test object placed at the scanner isocenter and at +2 cm, +4 cm, and +6 cm on the horizontal direction (x) for the evaluation of the radial spatial resolution and at ±5 cm on the vertical direction (y) for the evaluation of the spatial resolution in the tangential direction [4].

We focused on three acquisition protocols: head, abdomen/thorax, and inner ear. This last allows the acquisition at both standard (144×0.4 mm) and UHR (120×0.2 mm) modes. It should be noted that the UHR mode may require a higher radiation output to compensate for the increased noise associated with smaller detector pixel sizes, and therefore can be associated with a modest increase in patient dose compared to the standard mode [5]. Images were reconstructed using iterative algorithms. Both standard and vascular kernels were explored (Hr40, Hr60, Hr76, and Hv40, Hv60, Hv76 for the head; Br40, Br60, Br76, and Bv40, Bv60, Bv76 for the abdomen; Hr84, Hr89, and Hv84, Hv89 for the ear). The number indicated along the reconstruction method Br, Hr or Hv indicate the used recontruction kernel. The analysis of the images was performed via an automatic Python v. 3.9 script. The Point Spread Function (axial view of the wire) was integrated in the x-y direction to obtain the Line Spread Function (LSF), which was then normalized and Fourier-transformed to obtain the MTF.

## 3 Results

Spatial resolution is quantitatively evaluated in terms of the spatial frequencies corresponding to the 50% ($f_{50\%}$) and 10% ($f_{10\%}$) of the MTF curves. Increasing the kernel sharpness should improve the spatial resolution. This is well shown in figure 2, where the MTF curves for the abdominal protocol at increasing kernels are reported.

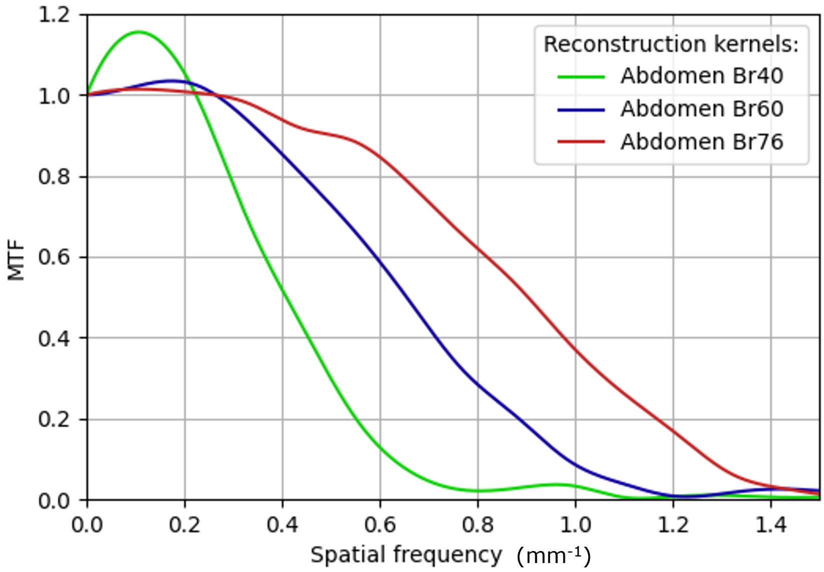


**Figure 2.** MTF for the abdominal protocol at increasing reconstruction kernels.

There is not a great evidence about the dependence of the spatial resolution on the specific type of reconstruction algorithm (whether standard or vascular): the comparison is summarized in figure 3 and table 1 (showing the $f_{50\%}$ and $f_{10\%}$) for the body kernel. The reconstruction kernel Br40 and Bv40 provoke an MTF enhancement at the low frequency, with an initial uptrend of the curves.

**Table 1.** $f_{50\%}$ and $f_{10\%}$ ($mm^{-1}$) for the three reconstruction kernels (comparing standard and vascular types) in the case of the abdominal acquisition protocols (wire at the isocenter).

| | Br40 | Bv40 | Br60 | Bv60 | Br76 | Bv76 |
|---|---|---|---|---|---|---|
| $f_{50\%}$ | 0.40 | 0.47 | 0.65 | 0.74 | 0.90 | 0.85 |
| $f_{10\%}$ | 0.62 | 0.67 | 0.98 | 1.14 | 1.27 | 1.27 |

Very similar results were obtained for the head acquisition protocol (figure 4), with $f_{50\%}$ ranging from 0.39 to 1.09 $mm^{-1}$ when increasing the kernel from Hr40 to Hr76.

The Inner Ear protocol was acquired since it allows both the standard and UHR modalities, which means a total z-collimation of 144×0.4 mm and 120×0.2 mm. This means that, in the first case, 140 detector rows with a z-thickness of 0.4 mm are used, while in the second case (UHR) 120 detector rows with a slice thickness of 0.2 mm (minimum possible for this scanner) are set. These values reflect a pixel size at the isocenter of 0.151×0.176 $mm^2$. We investigated how the UHR affected the spatial resolution, finding an improvement as shown in figure 5. For the standard collimation, the values obtained for $f_{50\%}$ and $f_{10\%}$ were 0.56 and 0.87 $mm^{-1}$, while for the UHR mode, they were 0.73 and 1.09 $mm^{-1}$.

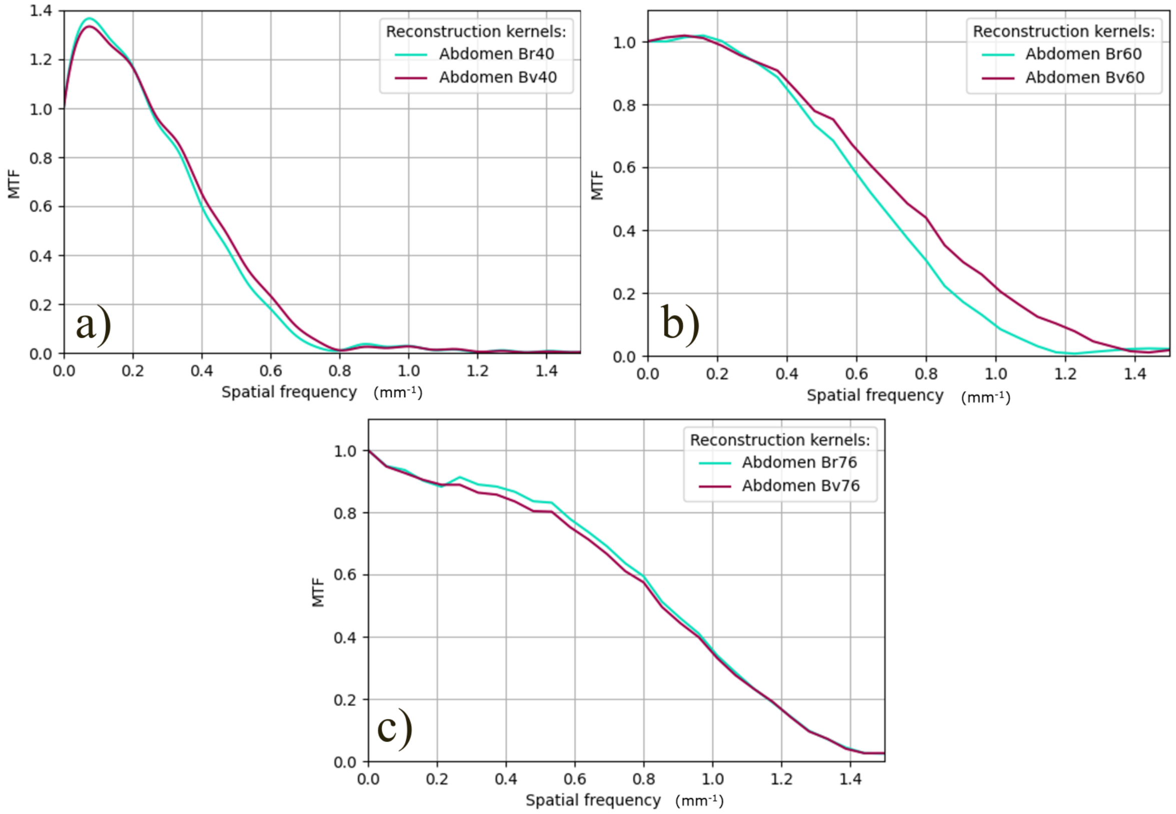


**Figure 3.** Comparison of the MTF curves between the standard and vascular kernels for the abdominal protocol. a) Br40 vs Bv40; b) Br60 vs Bv60; c) Br76 vs Bv76.

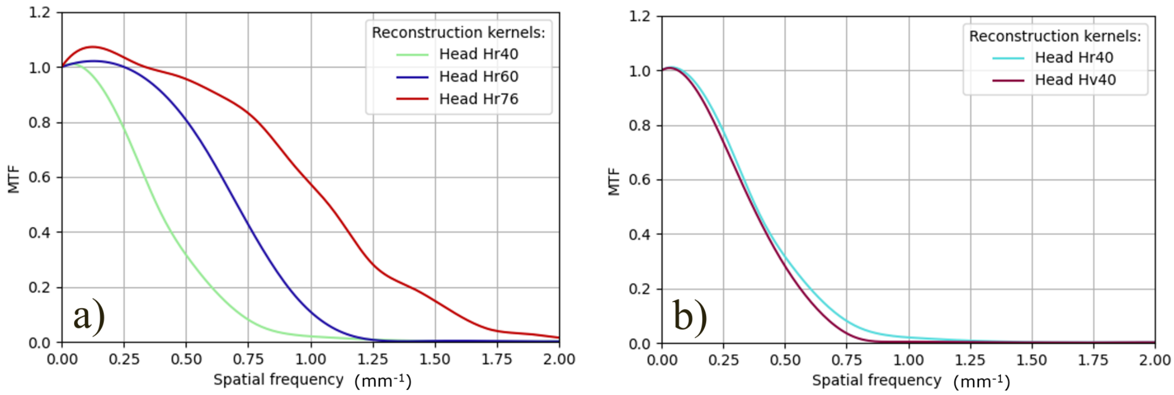


**Figure 4.** MTF results for the head acquisition protocol: a) Comparison at increasing kernels, b) Comparison of the standard and vascular kernels.

As seen in section 2, a characterization of the spatial resolution dependence along the radial and tangential directions of the gantry was provided by moving the wire phantom at different positions from the isocenter (figure 6). In both cases (x and y displacements), the MTF curves do not seem to have statistically significant differences from those acquired at the isocenter. To date, there are no papers in the literature showing, for a clinical PCCT scanner, the same methodologies proposed in this work. Previous works have proposed this method for conventional EID-CTs, varying the

2026 JINST 21 C01018

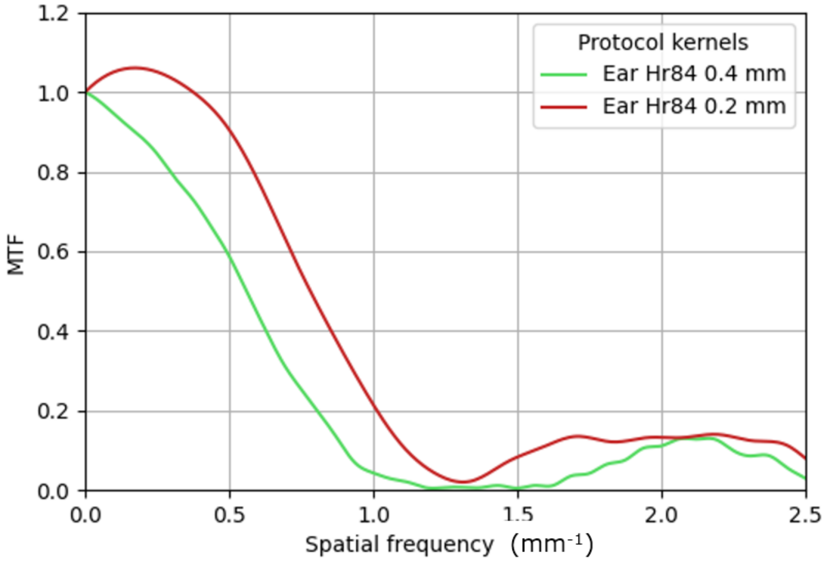


**Figure 5.** Inner Ear MTF curves for the Hr84 kernel. Comparison of the standard (144×0.4 mm) and UHR modes (120×0.2 mm).

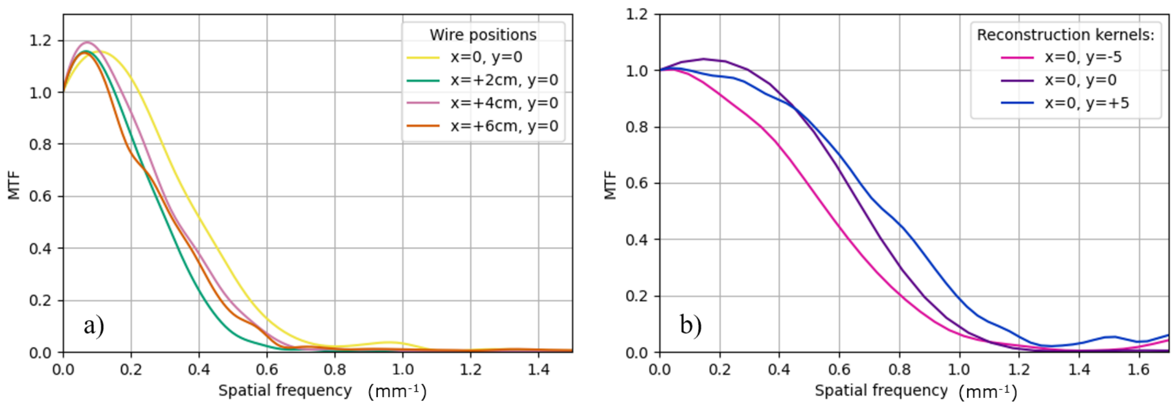


**Figure 6.** Characterization of the radial and tangential dependence of the MTF. a) Radial: acquisition positions at +2 cm, +4 cm, +6 cm on the horizontal axis; b) Tangential: acquisition positions at ±5 cm on the vertical axis.

type of scanners [6] or the detector element acquisition size and reconstruction kernels [7]. In these cases, the measured $f_{10\%}$ go from 0.63 to 0.78 $mm^{-1}$ [6], and from 1.16 to 1.98 $mm^{-1}$ [7] when varying the reconstruction kernel.

## 4 Conclusions

We provided a preliminary characterization of the spatial resolution of a Photon-Counting CT scanner, in terms of its Modulation Transfer Function. We demonstrated that the spatial resolution strongly depends on the chosen reconstruction algorithm and kernel (it increases, for all the investigated districts, when increasing the sharpness of the reconstructed image via a higher kernel), and also provided a proof that the Ultra-High resolution mode is associated with better values of the MTF than the standard mode (0.87 $mm^{-1}$ vs 1.09 $mm^{-1}$ for $f_{10\%}$). We did not observe any differences in the MTF curves when comparing the so-called standard and vascular reconstruction algorithms.

2026 JINST 21 C01018

Further investigations will be performed by means of a dedicated standard phantom to reduce the variability of the measurements and provide a comparison with other CT scanners.

## References


[1] P.C. Douek et al., *Clinical applications of photon-counting CT: A review of pioneer studies and a glimpse into the future*, *J. Clin. Investig.* **309** (2023) e222432.

[2] M. Tortora et al., *Spectral photon-counting computed tomography: A review on technical principles and clinical applications*, *Diagnostics* **13** (2023) 112.

[3] H. Fujita et al., *A simple method for determining the modulation transfer function in digital radiography*, *IEEE Trans. Med. Imag.* **11** (1992) 34.

[4] K. Yang, A.L. Kwan and J.M. Boone, *Computer modeling of the spatial resolution properties of a dedicated breast CT system*, *Med. Phys.* **34** (2007) 2059.

[5] F.S. Maddaloni et al., *Assessment of Image Quality Performance of a Photon-Counting Computed Tomography Scanner Approved for Whole-Body Clinical Applications*, *Sensors* **25** (2025) 7338.

[6] P. Barca et al., *A comprehensive assessment of physical image quality of five different scanners for head CT imaging as clinically used at a single hospital centre — A phantom study*, *PLoS One* **16** (2021) e0245374.

[7] A.M. Hernandez et al., *Location and direction dependence in the 3D MTF for a high-resolution CT system*, *Med. Phys.* **48** (2021) 2760.


2026 JINST 21 C01018